

ARTICLE OPEN



Removing forever chemicals via amphiphilic functionalized membranes

James K. Johnson¹, K. Michael Salerno¹, Danielle R. Schlesinger¹, Nam Q. Le¹, Jesse S. Ko¹ and Zhiyong Xia¹✉

Per- and poly-fluoroalkyl species (PFAS) remain ever-present drinking water contaminants. While some physical adsorption technologies for PFAS removal have been implemented on a large scale, they are limited by high cost and low effectiveness. In this work, an amphiphilic coating was developed and used to functionalize an aluminum oxide hydroxide membrane. Dynamic filtration of challenge water containing eighteen PFAS demonstrated >99% removal of eleven of eighteen PFAS as defined in EPA 537.1. Comparable performance was observed under gravity filtration conditions with >90% removal of fifteen of the eighteen PFAS. A comparison of breakthrough rates using amphiphilic silanes versus granular activated carbon (GAC), the commonly used filtration technology, was performed. Filters with the new amphiphilic coating outperformed GAC under dynamic filtration conditions by more than an order of magnitude for the perfluorooctanoic acid adsorption capacity and even greater for perfluorooctane sulfonic acid. Molecular dynamics simulations were used to compute the free energy, enthalpy, and entropy of interactions between coatings and six PFAS contaminants. Computed interaction free-energy (FE) values agree with experimental filtration performance across contaminants. The ability to use simulated FE values to predict filtration efficiency presents an opportunity for future in-silico rational design with overall reduced cost and development time.

npj Clean Water (2022)5:55; <https://doi.org/10.1038/s41545-022-00193-y>

INTRODUCTION

Per- and poly-fluoroalkyl species (PFAS) have emerged as widespread contaminants in drinking water^{1–3}. These highly fluorinated compounds persist in the environment as a result of the high chemical stability of the carbon–fluorine (C–F) bond and are therefore commonly referred to as “forever chemicals”^{4,5}. The environmental persistence and high water solubility of PFAS also leads to significant bioaccumulation, which is correlated with adverse health effects in human populations^{6–9}. The United States Environmental Protection Agency (EPA) has established a lifetime exposure drinking water limit for perfluorooctane sulfonic acid (PFOS) and perfluorooctanoic acid (PFOA) combined at 70 parts per trillion (ppt), a value exceeded at numerous locations in the United States and around the world¹⁰. While PFOA and PFOS are the two most common PFAS compounds, the broad PFAS family includes thousands of species with varying chain lengths, chain architecture, and charge¹¹. In particular, short-chain PFAS (perfluorocarboxylates with less than eight carbons and perfluorosulfonic acids with less than six carbons, such as perfluorobutanoic acid and perfluorobutane sulfonate) have proven to be significantly more difficult to sequester compared to longer chain PFAS^{12–15}.

The current state-of-the-art approach for PFAS removal focuses on physical adsorption techniques such as filtration via granular activated carbon (GAC) or ion exchange (IX) resins^{16–19}. Previous reports highlight limitations of GAC under high flux and poor performance in removing shorter chain PFAS species^{20–22}. In addition, GAC filter media can often be saturated by other contaminants, requiring frequent media replacement, leading to high filtration cost^{23,24}. The chemical reactivity of IX resins can be tailored to bind specific contaminant classes. This allows them to adsorb more PFAS than GAC under laboratory conditions, however, their costs are typically higher, limiting large-scale implementation^{25,26}.

Previously, we developed a cost-effective technology for removing heavy metal ions, PFOS, and PFOA using a silane-functionalized aluminum oxide hydroxide (γ -AlOOH) nanowhisker membrane (4603)^{27,28}. The previously developed amphiphilic silane coating contained a polar terminus to mitigate pressure drop and a fluorinated center to leverage the favorable fluorophilic C–F...F–C interaction for PFAS adsorption (F16-4PEG, Fig. 1). Since fluorinated species are hydrophobic, it was hypothesized that a silane containing a hydrophobic linker may also have utility in PFAS sequestration without the need for highly fluorinated building blocks. Here, we furthered our research and studied the efficacy of this technology by characterizing the breakthrough behavior, total contaminant adsorption, and filtration efficiency against PFAS with varying chain lengths, functionality, and concentrations. In addition, to understand differences in measured filtration efficiency, we employed Molecular Dynamics (MD) to model the interactions between six of the experimentally tested PFAS contaminants and modified F16-4PEG and H16-4PEG molecules in water. Metadynamics simulations were used to calculate the interaction free-energy (FE)^{29,30}, and results from MD simulations were compared quantitatively with experimental filtration efficiencies. In equilibrium, the FE of the interaction between the contaminant and filter is related to the filtration efficiency, this is often expressed in the literature as the partition coefficient^{31–34}. To understand differences in filtration efficiency as functions of PFAS and silane structure, interaction FE was also decomposed into entropic and enthalpic components. Results show that overall interactions are driven by entropy and solvation effects, explaining the difficulty in filtering relatively short PFAS molecules and suggesting future routes to better filtration.

¹The Johns Hopkins University Applied Physics Laboratory, 11100 Johns Hopkins Rd, Laurel, MD 20723, USA. ✉email: Zhiyong.Xia@jhuapl.edu

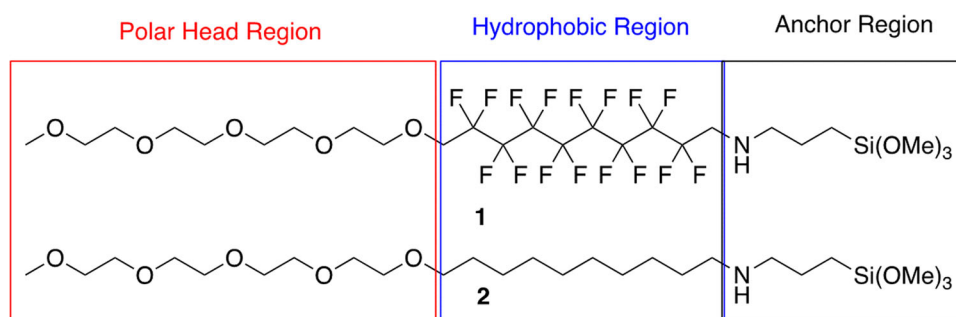


Fig. 1 Silane structures. Structures of amphiphilic silanes **1** (F16-4PEG) and **2** (H16-4PEG).

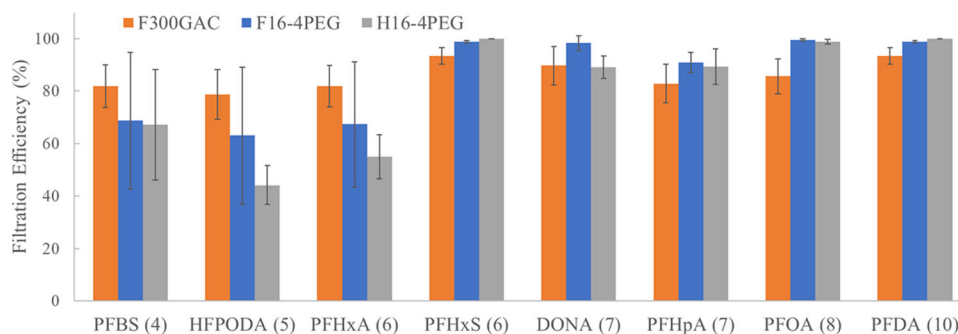


Fig. 2 Dynamic filtration experiment results. Percent removal of eight of the eighteen PFAS compounds under dynamic filtration of 100 ppt samples for the F300GAC, as well as F16-4PEG and H16-4PEG functionalized 4603 filters. The number of linear carbon atoms in each species is noted in parenthesis. For complete results see the Supplementary Table 1. Error bars represent the standard deviation for two independent experiments.

RESULTS

Dynamic filtration performance

A challenge water solution containing 100 ppt each of 18 PFAS species, identified in the EPA 537.1 (The 18 PFAS are perfluorohexanoic acid (PFHxA), perfluoroheptanoic acid (PFHpA), PFOA, perfluorononanoic acid (PFNA), perfluorodecanoic acid (PFDA), perfluorotridecanoic acid (PFTrDA), perfluorotetradecanoic acid (PFTeDA), perfluorobutanesulfonic acid (PFBS), perfluorohexanesulfonic acid (PFHxS), PFOS, *N*-ethylperfluorooctanesulfonamidoacetic acid (NEtFOSAA), *N*-methylperfluorooctanesulfonamidoacetic acid (NMeFOSAA), perfluorododecanoic acid (PFDoDA), hexafluoropropylene oxide dimer acid (HFPODA), 9-chlorohexadecafluoro-3-oxanone-1-sulfonic acid (9Cl-PF3ONS), 11-chloroeicosfluoro-3-oxaundecane-1-sulfonic acid (11Cl-PF3OUdS), 4,8-dioxa-3h-perfluorononanoic acid (DONA), and perfluoroundecanoic acid (PFUnDA), in deionized (DI) water was prepared. This concentration was identified based on previous reports of PFAS concentrations in waste water streams³⁵. Dynamic filtration tests were performed with 250 mL on three filtration media: (a) F16-4PEG functionalized 4603, (b) H16-4PEG functionalized 4603, and (c) Filtrasorb 300 GAC (F300GAC). Figure 2 shows the removal efficiency for the eight contaminants that were not completely removed by the F16-4PEG and H16-4PEG filters. For the other ten contaminants (PFOS, PFNA, NEtFOSAA, NMeFOSAA, PFDoDA, 9Cl-PF3OS, 11Cl-PF3OUdS, PFUnDA, perfluorotetradecanoic acid, perfluorotridecanoic acid) there is complete removal (>99.5%) by the F16-4PEG and H16-4PEG filters, while the F300GAC removal varies from 85–99%. See Supplementary Table 1 for complete results. Overall, for the 8 contaminants shown, the F16-4PEG and H16-4PEG functionalized filters performed as well as or better than the F300GAC, except for with short-chain PFAS like HFPODA, PFHxA, and PFBS. These short-chain PFAS have proven to be challenging to remove by other filtration methods and is likely

attributed to the lower affinity of the shorter chain PFAS to the filter media^{36,37}.

The filters were also challenged with the 18 PFAS solution at 750 ppt concentration per compound. At these PFAS concentration levels, the F16-4PEG functionalized filter shows >95% removal for all PFAS compounds except HFPODA (see Supplementary Fig. 1). Surprisingly, even the short-chain PFAS are removed with high efficiency. This is similarly noted in another study that used ppb and ppm levels of PFAS to evaluate an IX resin, which showed that competitive adsorption was not observed at PFAS concentrations ranging from 10 to 100 ppb³⁸. In comparison, the H16-4PEG displayed excellent removal of PFAS with more than six carbons and moderate removal of short-chain PFAS species. ADONA (4,8-dioxa-3h-perfluorononanoic acid) was also not completely removed since it is an ether acid with a high degree of oxygenation that might prevent effective interaction with the silanes. Conversely, PFNA, which has a similar side chain length without the oxygenation, is completely removed. This has been observed with other GAC and IX resin systems and is mainly a challenge for the shorter chain “ether acid” HFPODA^{39,40}.

Dynamic breakthrough behavior

To assess the breakthrough behavior, filters functionalized with both F16-4PEG and H16-4PEG were tested against challenge water containing both PFOA and PFOS with average concentration 415 ppt and 625 ppt, respectively, in DI water under a flux of 1223 L m⁻² h⁻¹. For comparison, a commercial Filtrasorb 300 GAC (F300GAC) was also tested. Breakthrough curves were generated from C/C₀ ratios as a function of collected volume of challenge water, where C is the effluent concentration (ng L⁻¹) and C₀ is the influent concentration (ng L⁻¹) (Fig. 3). For the F300GAC filter, at 15% breakthrough the volume of water filtered was estimated to be 30 mL (PFOA) and 50 mL (PFOS) with corresponding adsorbed mass of ~0.2 μg PFOA(g F300GAC)⁻¹ and 0.5 μg PFOS(g

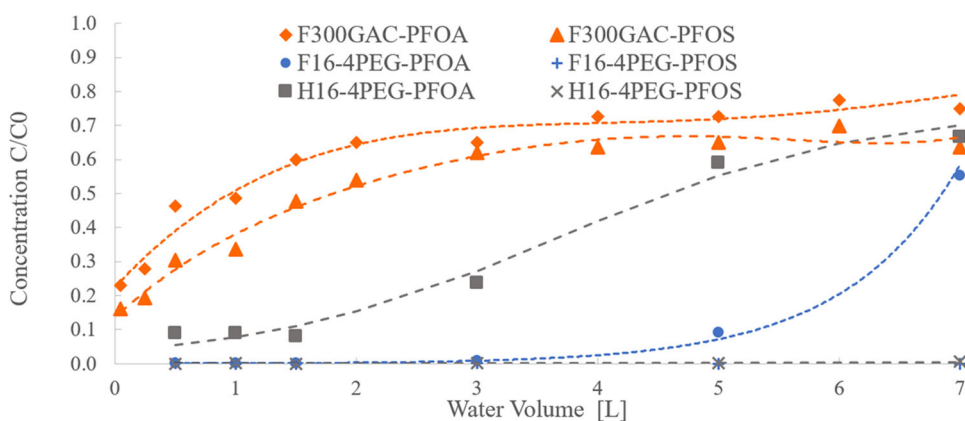


Fig. 3 Dynamic filtration breakthrough results. PFOA and PFOS breakthrough data showing C/C_0 for each filter substrate. Curves are guides for the eye. For the F300GAC errors are estimated to be 50% for both PFOA and PFOS. For the F16-4PEG filter errors are estimated to be 50% for PFOA and smaller than the symbol size for PFOS. For H16-4PEG the errors are estimated to be 50% before breakthrough of PFOA rising to 80% after breakthrough, and smaller than the symbol size for PFOS.

Table 1. Gravity filtration results.

	PFBS	HFPODA	PFHxA	PFHxS	PFHpA	DONA	PFOA	PFOS	PFNA	PFDA
F300GAC	97	95	95	97	96	96	94	99	98	99
F16-4PEG	83	62	68	100	94	97	93	100	100	99
H16-4PEG	73	73	69	100	94	93	97	100	100	100

The overall filtration efficiency of the F300GAC, F16-4PEG, and H16-4PEG for the nine contaminants that were not fully removed during gravity filtration. Values are the percent of contaminant filtered.

F300GAC)⁻¹²⁵. These values are estimates because the breakthrough concentration was surpassed at less than 50 mL volume. Under these high flux conditions, the F300GAC substrate did not provide removal below the EPA threshold of 70 ppt combined for PFOA and PFOS. The F16-4PEG functionalized medium displayed the highest adsorption capacity, with 15% breakthrough of PFOA after 5.2 L and $18 \mu\text{g PFOA}(\text{g F16-4PEG filter})^{-1}$ adsorbed mass. The H16-4PEG functionalized medium showed decreased performance compared to F16-4PEG with PFOA C/C_0 surpassing 15% at ~ 2.1 L, with about $7.5 \mu\text{g PFOA}(\text{g H16-4PEG filter})^{-1}$ adsorbed. For PFOS removal, filtration media functionalized with the F16-4PEG and H16-4PEG had similar performance, with little or no breakthrough at our largest measured water volumes. The difference in adsorption capacity could be due to the fact that PFOS contains one additional fluorinated carbon compared to PFOA making it slightly more hydrophobic²⁵. This difference is consistent with stronger interaction free energies for PFOS measured from MD reported in the SI. Comparing the masses of PFOA adsorbed at breakthrough, the F300GAC performed poorly relative to silane-functionalized substrates, with ~ 30 and 80 times less adsorbed mass at breakthrough for the H16-4PEG and F16-4PEG at $C/C_0 = 0.15$ respectively. PFOS breakthrough was not observed for the H16-4PEG or F16-4PEG filters, suggesting that they adsorb $>100\times$ contaminant mass than the F300GAC. This shows that F16-4PEG outperforms the other substrates for PFAS removal and that both the F16-4PEG and H16-4PEG have far higher adsorption capacity than the F300GAC medium.

Gravity filtration

Gravity filtration is commonly implemented for point-of-use filtration systems, such as a pitcher for drinking water. To assess the performance of the filter media under gravity filtration conditions, 1 L of challenge water containing 100 ppt of each of

the eighteen PFAS species in DI water was gravity filtered through a single 25 mm diameter filter with a flux of 85 (F300GAC) and $340 \text{ L m}^{-2} \text{ h}^{-1}$ (F16-4PEG and H16-4PEG). The variation in flow rate was the result of the low flow rate through the filter containing the F300GAC. The three filtration media performed very well for most contaminants, completely filtering 10 of the 18 PFAS species. Results for the contaminants that were not completely filtered are presented in Table 1. The F300GAC system outperformed F16-4PEG and H16-4PEG for the removal of short-chain PFAS. The slow filtration and long bed contact time are most likely the basis for the high removal of the PFAS from solution with GAC. However, these conditions are not ideal for large-scale processing. As in the dynamic filtration, the F16-4PEG and H16-4PEG silanes completely removed PFAS species with more than six carbon atoms, with modest removal of shorter PFAS like PFBS, HFPODA, and PFHxA.

Comparison of experimental and simulated MD results

Results from MD simulations quantify the FE, enthalpy, and entropy due to interactions between filter materials and contaminant molecules. Metadynamics simulations were used to compute the FE as a function of the center-of-mass separation between each filter molecule and each contaminant molecule^{29,30}. Typical interaction FE curves are shown in Supplementary Figs. 5 and 6. The most important feature of the FE curves is the depth of the FE minimum relative to the large-separation value. We refer to these values as the binding FE, denoted ΔG . For the contaminant filtration molecule pairs these values range from $-9 \text{ kJ}(\text{mol})^{-1}$ to $\sim -25 \text{ kJ}(\text{mol})^{-1}$, and can be read from Supplementary Figs. 5 and 6. The statistical uncertainties in the FE curves are $\sim \pm 1 \text{ kJ}(\text{mol})^{-1}$ for all contaminants except for the PFOS, which has error $\pm 1.9 \text{ kJ}(\text{mol})^{-1}$. Error bars represent the standard deviation from five independent metadynamics simulations.

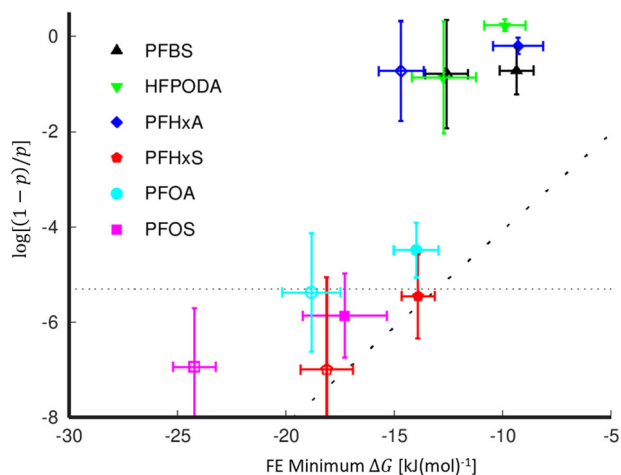


Fig. 4 Comparison of experimental and computational results.

The experimental filtration efficiency represented as $\log\left(\frac{1-p}{p}\right)$ versus the simulated FE minimum value ΔG . Experimental data for the 100 ppt dynamic filtration experiment are shown. Results for F16-4PEG are shown as open symbols while H16-4PEG results are closed symbols. Error bars represent the standard deviation of results from two independent experiments and the standard deviation of ΔG values from five independent metadynamics simulations.

The binding FE ΔG is related to experimental measurements of PFAS concentration by calculation of the partition coefficient^{31,33}. For a filter material and water in equilibrium, ΔG is related to the contaminant concentrations by $\Delta G = k_B T \log\left(\frac{c_w}{c_f}\right)$ where c_w is the contaminant concentration in the water and c_f is the contaminant concentration in the filter material. The contaminant concentration in the filter is proportional to the filtration efficiency $c_f \propto p$, while the contaminant concentration in water $c_w \propto (1-p)$. Altogether, the binding FE is related to the overall filtration efficiency p by

$$\Delta G = k_B T \log\left(\frac{1-p}{p}\right) + W \quad (1)$$

where the constant W varies with filter geometry, flow, and initial contaminant concentration. The simple relationship between p and ΔG in Eq. 1 will be modified as the filtered contaminant mass approaches saturation or breakthrough, and in that context other models to understand competitive binding by multiple molecules will be required^{41,42}.

Figure 4 compares experimental dynamic filtration efficiency data for 100 ppt contaminant sample water with simulated interaction FE values. The experimental data are recorded as $\log\left(\frac{1-p}{p}\right)$ and compared with ΔG from simulation. Error bars for the experimental data represent the standard deviation from duplicate experiments. The approximate experimental detection limit (<0.5 ppt) is indicated with a dashed horizontal line at ≈ -5.3 (100 ppt). Several contaminants are filtered to below this level, including the critically important PFOS and PFAS molecules, leading to large uncertainties for these species. Contaminants that are filtered completely are shown at a value of 0.25% filtration efficiency, the limit of detection for two experimental samples. The dashed black line represents a slope of $\frac{1}{k_B T}$ from Eq. 1 above. The data points generally follow this slope, however there is significant spread in the data points at or below the detection limit. Simulated ΔG values are compared with the 750 ppt dynamic filtration data in Supplementary Fig. 6.

To identify reasons for the differences in binding energies among contaminant-filter pairs, the binding free energies were

Table 2. Contributions to the simulated free energy.

Contaminant	Filter	ΔG (kJ/mol)	ΔH (kJ/mol)	$-T\Delta S$ (kJ/mol)
PFBS	F16-4PEG	-12.6 ± 1.0	21.6 ± 0.5	-34.2 ± 1.1
PFBS	H16-4PEG	-9.4 ± 0.3	23.8 ± 1.1	-33.2 ± 1.1
PFHxA	H16-4PEG	-9.3 ± 1.2	25.4 ± 0.5	-34.7 ± 1.3
PFHxS	H16-4PEG	-13.9 ± 0.8	25.2 ± 0.5	-39.1 ± 0.9
PFOA	H16-4PEG	-14.6 ± 1.0	25.3 ± 0.5	-39.9 ± 1.1
PFOS	H16-4PEG	-17.3 ± 1.9	28.5 ± 0.6	-45.8 ± 2.0

Total free energies of binding decomposed into enthalpic (ΔH) and entropic contributions ($-T\Delta S$) for selected contaminant-filter pairs, as estimated using molecular dynamics simulations.

decomposed into enthalpic and entropic contributions. The resulting values of ΔH are listed in Table 2, along with corresponding values of the total FE and the resulting estimated entropic contribution according to $\Delta G = \Delta H - T\Delta S$. Selected values of ΔH were also computed using MD simulations without metadynamics, and are reported in Supplementary Table 4. Those results are consistent with the values computed based on sampling from the metadynamics trajectories.

We draw two conclusions from the computed enthalpic and entropic contributions. First, the favorable free energies of binding $\Delta G < 0$ are driven in all cases by entropic contributions $-T\Delta S < 0$ rather than the enthalpies $\Delta H > 0$. Specific contributions to the enthalpy are reported in the Supplementary Table 5. Second, differences in ΔG among contaminant-filter pairs are also driven in all cases by $-T\Delta S$ rather than ΔH . For example, PFBS binds weakly to filters compared to PFOS ($\Delta G_{\text{PFBS}} > \Delta G_{\text{PFOS}}$) because its bound complex is much less stabilized by entropy ($-T\Delta S_{\text{PFBS}} > -T\Delta S_{\text{PFOS}}$), and that effect outweighs enthalpic contributions that actually favor PFBS ($\Delta H_{\text{PFBS}} < \Delta H_{\text{PFOS}}$). Taken together, these two conclusions suggest that while enthalpic considerations cannot be neglected, increasing the entropy of the bound filter-contaminant complex may be a more promising route to improve binding of especially challenging short-chain PFAS.

DISCUSSION

Filters functionalized with amphiphilic silanes proved highly effective in removing PFAS under high flux filtration conditions, with fluorinated silanes capable of removing eighteen PFAS species at high concentrations (750 ppt) and fifteen of the eighteen species at lower concentrations (100 ppt). Breakthrough studies further indicated effective removal with breakthrough over 5 L for PFOA and no detectable breakthrough for PFOS in the fluorinated silane. The non-fluorinated silane was also effective at adsorbing PFOS and PFOA, while GAC performed poorly in all cases. Gravity filtration demonstrated promising filter performance for the fluorinated silane with $>90\%$ removal for fifteen of the eighteen PFAS and $>99\%$ removal for twelve of the eighteen PFAS. MD simulations were performed to calculate the interaction FE between the six PFAS contaminant molecules and each of the two filter materials. Theoretical partition coefficients computed from interaction FEs were found to be consistent with experimental filtration efficiency measurements. The relationship between computed and experimentally measured quantities suggests the opportunity for rapid, in-silico development of filter materials. MD results were further analyzed to compute separate contributions to the FE from interaction enthalpy and entropy, which show that difficulty in filtering short PFAS molecules is largely driven by entropy. Our study indicates that amphiphilic silanes are a highly

efficient filter for dynamic PFAS filtration applications across a broad range of PFAS contaminants.

METHODS

Experimental methods

Detailed descriptions of all experiments, modeling, and analysis are described in the Supplementary Information. Dynamic filtration experiments were conducted using a previously reported method (with a flux of $1223 \text{ L m}^{-2} \text{ h}^{-1}$) based on the NSF protocols P248 and P473-2016^{28,43}. PFAS detection was conducted by solid phase extraction and liquid chromatography tandem mass spectrometry following EPA method 537.1, described in the Supplementary Methods PFAS Testing Section. Higher concentration PFAS dynamic filtration removal results are also described in Supplementary Methods Dynamic Filtration Experiments Section. A list of reagents and materials is described in the Supplementary Methods Reagents and Materials. The detailed experimental protocols for the synthesis of F16-4PEG and H16-4PEG are described in Supplementary Methods Silane Synthesis Section. The filter membrane functionalization and characterization (SEM/EDS, and BET adsorption isotherms) are described in Supplementary Methods Silane Functionalization and Materials Characterization Sections.

Modeling methods

MD simulations were used to calculate the FE and enthalpy of interactions between contaminant and filter molecules. Initial system states were parameterized using the automated topology builder tool, and constructed using the GROMACS tools^{44,45}. Due to difficulty in confirming silane parameters with multiple force-fields, an orthoformic group was substituted. The systems are comprised of $\sim 33,000$ atoms between filter and contaminant molecules, water, and salt. System parameterization and configuration details are in Supplementary Simulation initialization and interaction parameters, while details of initialization and equilibration are in Supplementary MD simulation parameters. After relaxation and equilibration, multiple-walker metadynamics MD simulations were executed using the colvars plugin to GROMACS^{45,46}. Four coupled simulations (walkers) of 100 ns are used simultaneously to construct the interaction FE in each independent computation. For each filter-contaminant pair five independent FE computations were performed, for a total of $2 \mu\text{s}$ simulation time per molecule pair. Details of the metadynamics method and parameters can be found in Supplementary Metadynamics Details and Parameters and references therein.

Binding enthalpies were calculated based on interaction energies from the metadynamics trajectories. Procedures were adapted from those previously used to analyze mechanisms of PFAS binding to clay surfaces³⁴. For selected contaminant-filter pairs, the enthalpy of binding was approximated as the difference in potential energy between bound and unbound states including interactions among contaminant, filter, and solvent. These potential energies were sampled every 20 ps over the trajectories of the metadynamics simulations. Bound and unbound states were identified based on the same collective distance coordinate: states with $0.35 \text{ nm} < d < 0.65 \text{ nm}$ were considered bound, and states with $d > 1.75 \text{ nm}$ were considered unbound. The mean energies of these sets of states were used to estimate the binding enthalpy as $\Delta H = H_{\text{bound}} - H_{\text{unbound}} \approx U_{\text{bound}} - U_{\text{unbound}}$. Uncertainties in these estimates of ΔH are reported as standard errors of the mean of the sampled potential energies.

DATA AVAILABILITY

The datasets generated during and/or analyzed during the current study are available from the corresponding author on reasonable request.

CODE AVAILABILITY

Simulation codes are freely available from the GROMACS website (www.gromacs.org) and via github (colvars.github.io).

Received: 6 March 2022; Accepted: 13 September 2022;

Published online: 04 October 2022

REFERENCES

- Ross, I. et al. A review of emerging technologies for remediation of PFASs. *Remediation* **28**, 101–126 (2018).
- Ahrens, L. & Bundschuh, M. Fate and effects of poly- and perfluoroalkyl substances in the aquatic environment: a review. *Environ. Toxicol. Chem.* **33**, 1921–1929 (2014).
- Garg, S. et al. A review on the sources, occurrence and health risks of per- and polyfluoroalkyl substances (PFAS) arising from the manufacture and disposal of electric and electronic products. *J. Water Process Eng.* **38**, 101638 (2020).
- Yu, Y. J. et al. Sequential C-F bond functionalizations of trifluoroacetamides and acetates via spin-center shifts. *Science* **371**, 1232–1240 (2021).
- Moody, C. A. & Field, J. A. Perfluorinated surfactants and the environmental implications of their use in fire-fighting foams. *Environ. Sci. Technol.* **34**, 3864–3870 (2000).
- Olsen, G. W. et al. Decline in perfluorooctanesulfonate and other polyfluoroalkyl chemicals in American Red Cross adult blood donors, 2000–2006. *Environ. Sci. Technol.* **42**, 4989–4995 (2008).
- Simon, J. A. et al. PFAS experts symposium: statements on regulatory policy, chemistry and analytics, toxicology, transport/fate, and remediation for per- and polyfluoroalkyl substances (PFAS) contamination issues. *Remediation* **29**, 31–48 (2019).
- Goodrum, P. E., Anderson, J. K., Luz, A. L. & Ansell, G. K. Application of a framework for grouping and mixtures toxicity assessment of PFAS: a closer examination of dose-additivity approaches. *Toxicol. Sci.* **179**, 262–278 (2021).
- Zeng, Z. et al. Assessing the human health risks of perfluorooctane sulfonate by in vivo and in vitro studies. *Environ. Int.* **126**, 598–610 (2019).
- EPA, 2016a. FACT SHEET PFOA & PFOS Drinking Water Health Advisories (EPA 800-F-16-003). Washington, DC, USA.
- Barzen-Hanson, K. A. et al. Discovery of 40 classes of per- and polyfluoroalkyl substances in historical aqueous film-forming foams (AFFFs) and AFFF-impacted groundwater. *Environ. Sci. Technol.* **51**, 2047–2057 (2017).
- U.S. EPA, Risk Management for Per- and Polyfluoroalkyl Substances (PFASs) under TSCA, <https://www.epa.gov/assessing-and-managing-chemicals-under-tsca/risk-management-and-polyfluoroalkyl-substances-pfass> (2017).
- Li, F. et al. Short-chain per- and polyfluoroalkyl substances in aquatic systems: occurrence, impacts and treatment. *Chem. Eng. J.* **380**, 122506 (2020).
- Ateia, M., Maroli, A., Tharayil, N. & Karanfil, T. The overlooked short- and ultrashort-chain poly- and perfluorinated substances: a review. *Chemosphere* **220**, 866–882 (2019).
- Stebel, E. K. et al. Absorption of short-chain to long-chain perfluoroalkyl substances using swellable organically modified silica. *Environ. Sci. Water Res. Technol.* **5**, 1854 (2019).
- Lu, D., Sha, S., Luo, J., Huang, Z. & Zhang, J. X. Treatment train approaches for the remediation of per- and polyfluoroalkyl substances (PFAS): a critical review. *J. Haz. Mat.* **386**, 121963 (2020).
- Militao, I. M., Roddick, F. A., Bergamasco, R. & Fan, L. Removing PFAS from aquatic systems using natural and renewable material-based adsorbents: a review. *J. Environ. Chem. Eng.* **9**, 105271 (2021).
- Fang, Y. et al. Removal of per- and polyfluoroalkyl substances (PFASs) in aqueous film-forming foam (AFFF) using ion-exchange and nonionic resins. *Environ. Sci. Technol.* **55**, 5001–5011 (2021).
- Woodard, S., Berry, J. & Newman, B. Ion exchange resin for PFAS removal and pilot test comparison to GAC. *Remediation* **27**, 19–27 (2017).
- Xiao, X., Ulrich, B. A., Chen, B. & Higgins, C. P. Sorption of poly- and perfluoroalkyl substances (PFASs) relevant to aqueous film forming foam (AFFF)-impacted groundwater by biochars and activated carbon. *Environ. Sci. Technol.* **51**, 6342–6351 (2017).
- McCleaf, P. et al. Removal efficiency of multiple poly- and perfluoroalkyl substances (PFASs) in drinking water using granular activated carbon (GAC) and anion exchange (AE) column tests. *Water Res.* **120**, 77–87 (2017).
- Appleman, T. D. et al. Treatment of poly- and perfluoroalkyl substances in U.S. full-scale water treatment systems. *Water Res.* **51**, 246–255 (2014).
- Belkouteb, N., Franke, V., McCleaf, P., Köhler, S. & Ahrens, L. Removal of per- and polyfluoroalkyl substances (PFASs) in a full-scale drinking water treatment plant: Long-term performance of granular activated carbon (GAC) and influence of flow-rate. *Water Res.* **182**, 115913 (2020).

24. Franke, V. et al. The price of really clean water: combining nanofiltration with granular activated carbon and anion exchange resins for the removal of per- and polyfluoroalkyl substances (PFASs) in drinking water production. *ACS EST Water* **1**, 782–795 (2021).
25. Liu, C. J., Werner, D. & Bellona, C. Removal of per- and polyfluoroalkyl substances (PFASs) from contaminated groundwater using granular activated carbon: a pilot-scale study with breakthrough modeling. *Environ. Sci. Water Res. Technol.* **5**, 1844–1853 (2019).
26. Dixit, F., Dutta, R., Barbeau, B., Berube, P. & Mohseni, M. PFAS removal by ion exchange resins: a review. *Chemosphere* **272**, 129777 (2021).
27. Xia, Z., Baird, L., Zimmerman, N. & Yeager, M. Heavy metal ion removal by thiol functionalized aluminum oxide hydroxide nanowhiskers. *Appl. Surf. Sci.* **416**, 565–573 (2017).
28. Johnson, J. K., Hoffman, C. M., Smith, D. A. & Xia, Z. Advanced filtration membranes for the removal of perfluoroalkyl species from water. *ACS Omega* **4**, 8001–8006 (2019).
29. Raiteri, P., Laio, A., Gervasio, F. L., Micheletti, C. & Parrinello, M. Efficient reconstruction of complex free energy landscapes by multiple walkers metadynamics. *J. Phys. Chem. B* **110**, 3533–3539 (2006).
30. Laio, A. & Parrinello, M. Escaping free-energy minima. *Proc. Natl Acad. Sci. USA* **99**, 12562–12566 (2002).
31. Ruelle, P. The *n*-octanol and *n*-hexane/water partition coefficient of environmentally relevant chemicals predicted from the mobile order/disorder (MOD) thermodynamics. *Chemosphere* **40**, 457–512 (2000).
32. Willemsen, J. A. R. et al. Molecular dynamics simulations of the adsorption of phthalate esters on smectite clay surfaces. *J. Phys. Chem. C* **123**, 13624–13636 (2019).
33. Matos, G. D. R. et al. Approaches for calculating solvation free energies and enthalpies demonstrated with an update of the freesolv database. *J. Chem. Eng. Data* **62**, 1559–1569 (2017).
34. Willemsen, J. A. R. & Bourg, I. C. Molecular dynamics simulation of the adsorption of per- and polyfluoroalkyl substances (PFASs) on smectite clay. *J. Colloid Interface Sci.* **2021**, 337–346.
35. Kurwadkar, S. et al. Per- and polyfluoroalkyl substances in water and wastewater: a critical review of their global occurrence and distribution. *Sci. Total Environ.* **809**, 151003 (2022).
36. Herkert, N. J. et al. Assessing the effectiveness of point-of-use residential drinking water filters for perfluoroalkyl substances (PFASs). *Environ. Sci. Technol. Lett.* **7**, 178–184 (2020).
37. Ateia, M. et al. Cationic polymer for selective removal of GenX and short-chain PFAS from surface waters and wastewaters at ng/L levels. *Water Res.* **163**, 114874 (2019).
38. Liu, C., Chu, J., Cápiro, N. L., Fortner, J. D. & Pennell, K. D. In-situ sequestration of perfluoroalkyl substances using polymer-stabilized ion exchange resin. *J. Haz. Mat.* **422**, 126960 (2022).
39. Wang, W. et al. Adsorption behavior and mechanism of emerging perfluoro-2-propoxypropanoic acid (GenX) on activated carbons and resins. *Chem. Eng. J.* **364**, 132–138 (2019).
40. Dixit, F., Barbeau, B., Mostafavi, S. G. & Mohseni, M. Efficient removal of GenX (HFPO-DA) and other perfluorinated ether acids from drinking and recycled waters using anion exchange resins. *J. Haz. Mat.* **384**, 121261 (2020).
41. Langmuir, I. The adsorption of gases on plane surfaces of glass, mica, and platinum. *J. Am. Chem. Soc.* **40**, 1361–1403 (1918).
42. Brunauer, S., Emmett, P. H. & Teller, E. Adsorption of gases in multimolecular layers. *J. Am. Chem. Soc.* **60**, 309–319 (1938).
43. EPA. EPA Method 537.1. **1** (2009), 1–50 (2018).
44. Malde, A. K. et al. An Automated force field Topology Builder (ATB) and repository: version 1.0. *J. Chem. Theory Comput.* **7**, 4026–4037 (2011).
45. Hess, B., Kutzner, C., Van Der Spoel, D. & Lindahl, E. GROMACS 4: algorithms for highly efficient, load-balanced, and scalable molecular simulation. *J. Chem. Theory Comput.* **4**, 435–447 (2008).
46. Fiorin, G., Klein, M. L. & Hénin, J. Using collective variables to drive molecular dynamics simulations. *Mol. Phys.* **111**, 3345–3362 (2013).

ACKNOWLEDGEMENTS

The authors acknowledge the support from the Independent Research and Development (IRAD) Fund from the Research and Exploratory Development Mission Area of the Johns Hopkins University Applied Physics Laboratory. The authors also thank Dr. Tim Montalbano for the assistance with SEM and Mr. Collin McDermott for the gravity filtration testing.

AUTHOR CONTRIBUTIONS

The manuscript was written with the contributions of all authors. All authors have given approval for the final version of the manuscript. Z.X., J.K.J., and D.R.S. designed and executed the experiments. K.M.S. and N.Q.L. performed modeling and analysis. J.S.K. provided materials analysis and characterization.

COMPETING INTERESTS

The authors declare no competing interests. The following competing financial interest includes a patent application that has been filed for this work by authors Z.X., J.K.J., D.R.S., J.S.K., and N.Q.L.

ADDITIONAL INFORMATION

Supplementary information The online version contains supplementary material available at <https://doi.org/10.1038/s41545-022-00193-y>.

Correspondence and requests for materials should be addressed to Zhiyong Xia.

Reprints and permission information is available at <http://www.nature.com/reprints>

Publisher's note Springer Nature remains neutral with regard to jurisdictional claims in published maps and institutional affiliations.



Open Access This article is licensed under a Creative Commons Attribution 4.0 International License, which permits use, sharing, adaptation, distribution and reproduction in any medium or format, as long as you give appropriate credit to the original author(s) and the source, provide a link to the Creative Commons license, and indicate if changes were made. The images or other third party material in this article are included in the article's Creative Commons license, unless indicated otherwise in a credit line to the material. If material is not included in the article's Creative Commons license and your intended use is not permitted by statutory regulation or exceeds the permitted use, you will need to obtain permission directly from the copyright holder. To view a copy of this license, visit <http://creativecommons.org/licenses/by/4.0/>.

© The Author(s) 2022